Title

A Noncanonical Metal Center Drives the Activity of the Sediminispirochaeta smaragdinae Metallo-β-lactamase SPS-1

Journal

Biochemistry, 57(35)

ISSN

0006-2960

Authors

Cheng, Zishuo

VanPelt, Jamie

Bergstrom, Alexander

et al.

Publication Date

2018-09-04

DOI

10.1021/acs.biochem.8b00728

Peer reviewed

Biochemistry

Article

Cite This: *Biochemistry* 2018, 57, 5218−5229

pubs.acs.org/biochemistry

A Noncanonical Metal Center Drives the Activity of the *Sediminispirochaeta smaragdinae* Metallo-β-lactamase SPS-1

Zishuo Cheng,[†] Jamie VanPelt,[†] Alexander Bergstrom,[†] Christopher Bethel,[‡] Andrew Katko,[†] Callie Miller,[†] Kelly Mason,[†] Erin Cumming,[†] Huan Zhang,[†] Robert L. Kimble,[†] Sarah Fullington,[†] Stacey Lowery Bretz,[†] Jay C. Nix,[∥] Robert A. Bonomo,[‡,§] David L. Tierney,[†] Richard C. Page,*[,†] and Michael W. Crowder*[,†]

[†]Department of Chemistry and Biochemistry, Miami University, 651 East High Street, 160 Hughes Laboratories, Oxford, Ohio 45056, United States

[‡]Research Service, Louis Stokes Cleveland Department of Veterans Affairs Medical Center, Cleveland, Ohio 44106, United States

[§]Departments of Medicine, Pharmacology, Molecular Biology and Microbiology, Biochemistry, Proteomics, and Bioinformatics and CWRU-Cleveland VAMC Center for Antimicrobial Resistance and Epidemiology, Case Western Reserve University, Cleveland, Ohio 44106, United States

[∥]Molecular Biology Consortium, Beamline 4.2.2, Advanced Light Source, Lawrence Berkeley National Laboratory, Berkeley, California 94720, United States

Supporting Information

ABSTRACT: In an effort to evaluate whether a recently reported putative metallo-β-lactamase (MβL) contains a novel MβL active site, SPS-1 from *Sediminispirochaeta smaragdinae* was overexpressed, purified, and characterized using spectroscopic and crystallographic studies. Metal analyses demonstrate that recombinant SPS-1 binds nearly 2 equiv of Zn(II), and steady-state kinetic studies show that the enzyme hydrolyzes carbapenems and certain cephalosporins but not β-lactam substrates with bulky substituents at the 6/7 position. Spectroscopic studies of Co(II)-substituted SPS-1 suggest a novel metal center in SPS-1, with a reduced level of spin coupling between the metal ions and a novel Zn_1 metal binding site. This site was confirmed with a crystal structure of the enzyme. The structure shows a Zn_2 site that is similar to that in NDM-1 and other subclass B1 MβLs; however, the Zn_1 metal ion is coordinated by two histidine residues and a water molecule, which is held in position by a hydrogen bond network. The Zn_1 metal is displaced nearly 1 Å from the position reported in other MβLs. The structure also shows extended helices above the active site, which create a binding pocket that precludes the binding of substrates with large, bulky substituents at the 6/7 position of β-lactam antibiotics. This study reveals a novel metal binding site in MβLs and suggests that the targeting of metal binding sites in MβLs with inhibitors is now more challenging with the identification of this new MβL.

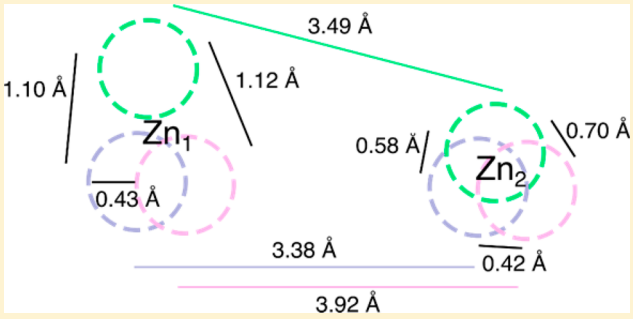

β-Lactam antibiotics, such as penicillins, cephalosporins, and carbapenems, have long served as treatments for bacterial infections by inactivation of bacterial transpeptidases. These compounds constitute the largest class of clinically available antibiotics. In response to wide use, and overuse, of β-lactam-containing drugs, bacteria have evolved to produce β-lactamases that hydrolyze the β-lactam bond and render the antibiotics inactive.

Of the four classes of β-lactamases (A−D), only class B enzymes require one or two Zn(II) ions, rather than an active site serine, for catalysis and are termed metallo-β-lactamases (MβLs).[1−3] MβLs adopt an αββα fold, and among the three subclasses (B1−B3), B1 and B3 MβLs generally contain a dinuclear Zn(II) active site, while B2 MβLs are active with mononuclear Zn(II) sites. The B1 MβLs coordinate one Zn(II) (in the Zn_1 site) with three histidine residues, while the Zn(II) in the Zn_2 site is bound to one cysteine, one aspartate, one histidine, and a terminally bound solvent molecule. The Zn(II) ions are bridged by a solvent molecule, resulting in a Zn−Zn distance of 3.3−3.9 Å.[2,4] The B3 MβLs possess the same Zn_1 site as the B1 MβLs; however, in the Zn_2 site, the cysteine ligand is replaced with an additional His residue. Subclass B1 contains the largest number of clinically relevant MβLs, including VIMs (Verona integrin-encoded MβL), IMPs (imipenemase), and NDMs (New Delhi MβL). Most recent studies have focused on MβLs found in pathogenic strains;

Received: July 6, 2018
Revised: August 8, 2018
Published: August 14, 2018

DOI: 10.1021/acs.biochem.8b00728
Biochemistry 2018, 57, 5218−5229

however, the risk of transfer of antibiotic resistance determinants from a nonpathogenic strain to a more clinically relevant organism necessitates the need to study MβLs not yet found in known human pathogens.[5]

Recently, with the use of a Markov model and a bioinformatic study, Berglund et al. identified 279 unique, potential subclass B1 MβL genes, and 76 of the corresponding gene products were novel and able to hydrolyze imipenem.[6] One gene, *SPS-1*, was found in the bacterium *Sediminispirochaeta smaragdinae* (NCBI reference sequence WP_013255389.1). *S. smaragdinae* strain SEBR 4228^T was discovered in a water sample near a Congo offshore oilfield.[7] SEBR 4228^T is a Gram-negative, chemoorganotrophic, and anaerobic bacterium that adopts a spiral, corkscrew-like structure. This organism is halophilic and able to grow in high-salt environments. SPS-1 was predicted to be a MβL; however, SPS-1 lacked the typical H-X-H-X-D motif found in all MβLs except the B2 MβLs. In SPS-1, the first consensus histidine residue was substituted with a glycine.[6] In an effort to determine if SPS-1 is indeed a MβL and how the histidine to glycine substitution affected the consensus Zn_1 site, we cloned, overexpressed, and purified the enzyme and characterized the recombinant protein via kinetic, spectroscopic, and crystallographic studies.

MATERIALS AND METHODS

Phylogenetic Analysis of SPS-1. The protein sequences of selective class B β-lactamases (MβLs), as well as SPS-1, were downloaded from the NCBI GenBank and analyzed using Phylogeny.fr (http://www.phylogeny.fr/).[8,9]

Cloning, Overexpression, and Purification of SPS-1. A codon-optimized SPS-1 sequence (residues 32−276) fused with an N-terminal tobacco etch virus (TEV) cleavage site was synthesized by Genscript Biotech Corp. The synthesized fragment was subcloned into pET28a between the *Nde*I and *Xho*I restriction sites. The resulting overexpression plasmid, pET28a-SPS-1, was transformed into *Escherichia coli* EXPRESS BL21(DE3) Chemically Competent cells (Lucigen). A single colony was transferred into 50 mL of lysogeny broth (LB) containing 50 μg/mL kanamycin, and the culture was shaken overnight at 37 °C. The overnight culture (10 mL) was used to inoculate four 1 L LB cultures containing 50 μg/mL kanamycin. The resulting culture was grown at 37 °C with a shaking speed of 220 rpm until an OD_{600} of 0.6 was reached. Protein production was induced by addition of isopropyl β-D-1-thiogalactopyranoside (IPTG) to a final concentration of 500 μM. At the time of induction, cultures were supplemented with Zn(II) with addition of $ZnCl_2$ to a concentration of 100 μM. Cultures were shaken overnight at 18 °C and then harvested by centrifugation for 10 min at 8000*g*. Cell pellets were resuspended in 50 mL of 50 mM HEPES (pH 7.5) containing 500 mM NaCl. Cells were lysed by passing the mixture two times through a French press at a pressure between 15000 and 20000 psi. The insoluble components were removed by centrifugation for 1 h at 32000*g*. The supernatant was loaded onto a HisTrap HP (5 mL, GE) column and washed with 10 volumes of wash buffer containing 50 mM HEPES (pH 7.5), 500 mM NaCl, and 50 mM imidazole. Bound proteins were eluted using elution buffer (wash buffer with 500 mM imidazole). TEV protease was added at a 1:100 (w/w) ratio to SPS-1. The eluted proteins were dialyzed against 1 L of 50 mM HEPES (pH 7.5) containing 500 mM NaCl. After overnight dialysis, the truncated SPS-1 protein was repurified by being passed through a HisTrap column, which removed the His_6-TEV and His_6 tag.

Purified recombinant SPS-1 (before and after TEV digestion) was analyzed by sodium dodecyl sulfate−polyacrylamide gel electrophoresis (SDS−PAGE) using a Fisher EZ-Gel solution (12.5%), a Mini-PROTEAN System (Bio-Rad Laboratories), and Coomassie Blue stain. Protein concentrations were determined by ultraviolet−visible (UV−vis) absorbance at 280 nm using an ε_{280} of 35535 M^{-1} cm^{-1} for the SPS-1 protein containing the His_6 tag and an ε_{280} of 34045 M^{-1} cm^{-1} for the SPS-1 protein without the His_6 tag. These extinction coefficients were calculated using ExPASY ProtParam.[10]

Matrix-Assisted Laser Desorption Ionization Time-of-Flight (MALDI-TOF) Mass Spectrometry. After dialysis against 10 mM ammonium acetate (pH 7.5), 30 μM tag-free SPS-1 was mixed with a sinapinic acid matrix at a ratio of 1:1. The resulting sample was analyzed using a Bruker AutoFlex MALDI-TOF mass spectrometer.[11]

Fluorescence Spectroscopy. Fluorescence emission spectra of SPS-1 were recorded on a PerkinElmer luminescence spectrometer (model LS-55) using 2 μM SPS-1 in 50 mM HEPES (pH 7.5). Spectra were acquired using an excitation wavelength of 280 nm and an emission spectrum window from 300 to 500 nm.

Metal Analyses. The zinc contents of purified SPS-1 samples were determined using a PerkinElmer Optima 7300V inductively coupled plasma spectrometer with optical emission spectroscopy (ICP-OES) detection. Protein samples, used without modification after purification, were diluted to 5 μM with 10 mM ammonium acetate (pH 7.5). Calibration curves were generated using serial dilutions of FisherBrand Zn metal standard ranging from 0 to 16 μM, and the emission line at 202.548 nm was chosen for zinc.

Steady-State Kinetics. Steady-state kinetic studies were performed using a Synergy HT Multi-Mode Microplate Reader (Biotek) at 37 °C in 50 mM HEPES (pH 7.5) containing 150 mM NaCl and 10 μM $ZnCl_2$. The following changes in molar absorptivity ($\Delta\varepsilon$, M^{-1} cm^{-1}) were used to quantitate products: chromacef, $\Delta\varepsilon_{442}$ = 18600; cephalothin, $\Delta\varepsilon_{265}$ = −8790; imipenem, $\Delta\varepsilon_{300}$ = −9000; meropenem, $\Delta\varepsilon_{293}$ = −7600; ampicillin, $\Delta\varepsilon_{235}$ = −809; penicillin G, $\Delta\varepsilon_{235}$ = −936; cefuroxime, $\Delta\varepsilon_{260}$ = −5860; and cephalexin, $\Delta\varepsilon_{260}$ = −7750.[12] Initial rates (within 18 s) versus substrate concentrations were fitted to the Michaelis−Menten equation to determine the steady-kinetic constants K_m and k_{cat} using Prism 7 (Graphpad Software).

Isothermal Titration Calorimetry. Isothermal titration calorimetry (ITC) experiments were performed using a Nano ITC System (TA Instruments-Waters LLC) with a 500 μL cell. All experiments were performed at 25 °C. SPS-1 and NDM-1 were prepared by diluting the stock solutions with 20 mM HEPES (pH 7.5) containing 150 mM NaCl. L-Captopril (Acros Organics) was dissolved in the same buffer. The ITC cell was filled with 50 μM NDM-1 or SPS-1 (300 μL), and the enzyme solutions were titrated with 250 μM captopril. The injection volume was 50 μL, and the time between two injections was 210 s. K_d values were determined by using NanoAnalyze (TA Instruments-Waters LLC).

Preparation of Metal-Free Proteins. Metal-free forms of SPS-1 and NDM-1 were prepared through metal chelation. Each purified protein (diluted to 50 μM in 20 mL) was placed in a 10 kDa molecular weight cutoff dialysis bag. These

DOI: 10.1021/acs.biochem.8b00728
Biochemistry 2018, 57, 5218−5229

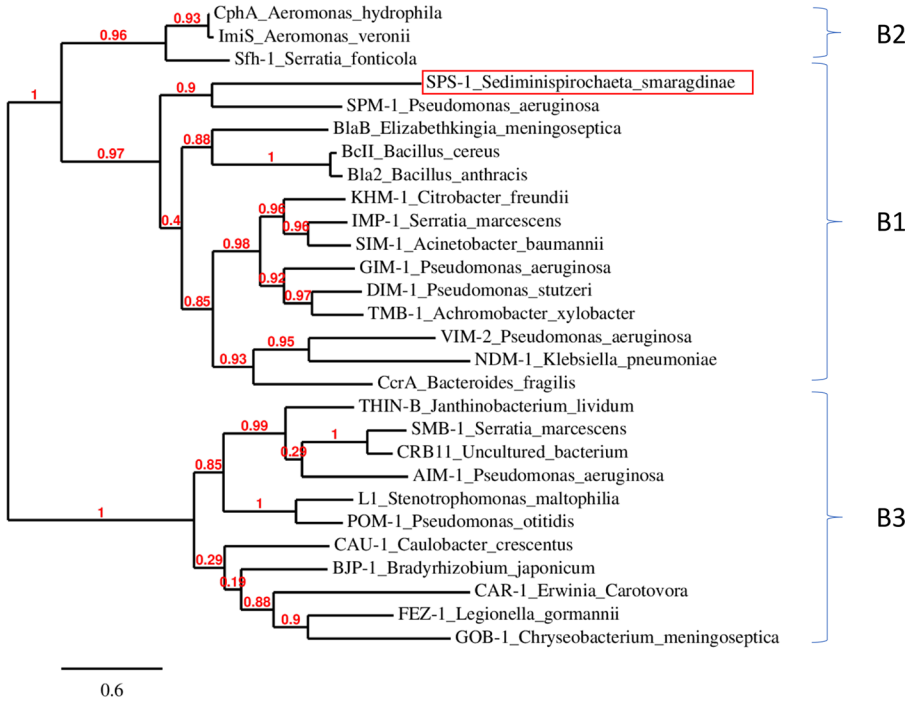

Figure 1. Phylogenetic tree of class B metallo-β-lactamase sequences. The protein sequences of SPS-1 and other selective metallo-β-lactamase were downloaded and analyzed by Phylogeny.fr. The sequence include SPS-1 (WP_013255389.1), BcII (M11189), CcrA (M63556), IMP-1 (S71932), VIM-2 (AF191564), BlaB (AF189298), SPM-1 (AY341249), NDM-1 (JN420336), GIM-1 (AJ620678), SIM-1 (AY887066), DIM-1 (GU323019), TMB-1 (FR771847), Bla2 (CP001598), KHM-1 (AB364006), CphA (X57102), Sfh-1 (AF197943), ImiS (Y01415), L1 (AB294542), FEZ-1 (Y17896), BJP-1 (NP772870), AIM-1 (AM998375), THIN-B (CAC33832), GOB-1 (ABO21417), CAU-1 (CAC87665), CAR-1 (Q6D395), SMB-1 (AB636283), POM-1 (ADC79555), and CRB11 (ACS83724). The line segment with the number 0.6 shows the length of the branch that represents an amount of genetic change of 0.6.

samples were dialyzed versus dialysis buffers for 4 h at 4 °C before changing to the subsequent dialysis buffer to include a series of five dialysis steps: first, two changes of 50 mM HEPES (pH 6.8) containing 150 mM NaCl with 2 mM EDTA and, then, three changes of 50 mM HEPES (pH 6.8) containing 150 mM NaCl. The resulting metal-free enzymes were analyzed by using SDS−PAGE and UV−vis and concentrated by using an Amicon Ultra 15 mL centrifugal filter (10K).

UV−vis Spectroscopy. Metal-free SPS-1 and NDM-1 were diluted to 300 μM with 50 mM HEPES (pH 6.8) containing 150 mM NaCl and 1 mM tris(2-carboxyethyl)-phosphine (TCEP). One or two molar equivalents of $CoCl_2$ was added to the protein samples from a 50 mM stock solution. The resulting mono-Co(II)-substituted or di-Co(II)-substituted protein samples were placed in 500 μL quartz cuvettes, and UV−vis spectra were recorded on a PerkinElmer Lambda 750 UV/vis/NIR spectrometer that measured the absorbance between 300 and 700 nm at 25 °C. The blank spectrum of 300 μM apo-SPS-1 or apo-NDM-1 in 50 mM HEPES (pH 6.8) containing 150 mM NaCl and 1 mM TCEP was used to generate difference spectra. All data were normalized to the absorbance at 700 nm.

NMR Spectroscopy. Metal-free SPS-1 was concentrated to ∼0.5 mM with an AmiconUltra-15 centrifugal unit and an Ultracel-10 membrane. To the concentrated protein was added 2 equiv of $CoCl_2$ in the buffer containing 50 mM HEPES (pH 6.8), 150 mM NaCl, and 10% (v/v) D_2O. Spectra were recorded at 292 K on a Bruker ASX300 (BBI probe) NMR spectrometer operating at a frequency of 300.16 MHz. Spectra were collected using a frequency switching method, applying a long low-power (270 ms) pulse centered at the water frequency, followed by a high-power 3 μs pulse centered at either 200 or 90 ppm to ensure all resonances were detected.[13] This method allowed for suppression of the water signal with enhancement of severely hyperfine-shifted resonances. Spectra consisted of 120000 transients of 16K data points over a 333 ppm spectral window (τ_{aq} ∼ 51 ms). Signal averaging took ∼12 h per spectrum.

EPR Spectroscopy. EPR samples containing SPS-1 or NDM-1 included approximately 10% (v/v) glycerol as a glassing agent. Samples were loaded into EPR tubes and degassed by repeated evacuation/purging with N_2 prior to data collection. Spectra were recorded on a Bruker EMX EPR spectrometer, equipped with an ER4116-DM dual-mode resonator (9.37 GHz, parallel; 9.62 GHz, perpendicular). The data in EPR figures were scaled so that the *X*-axes matched (perpendicular mode field values were scaled by 9.37/9.62). The temperature was controlled using an Oxford ESR900 cryostat and temperature controller (4.5 K). Other spectral conditions included a microwave power of 0.2 mW, a field modulation of 10 G (100 kHz), a receiver gain of 10^4, and a time constant/conversion time of 41 ms.

Crystallization, Diffraction Data Collection, and Structural Refinement. SPS-1 was crystallized using 96-well sitting drop vapor diffusion screens prepared using a Phoenix crystallization robot (Art Robbins). The sitting drops contained 400 nL of 1.45 mM SPS-1 and 400 nL of the crystallization condition. Six crystallization screens were used: MCSG 1−4 by Microlytic and JCSG and PACT++ by JBScreen. Diffraction quality crystals formed within 2 weeks under a condition consisting of 0.2 M magnesium chloride, 0.1 M sodium cacodylate (pH 6.5), and 50% (v/v) PEG 200. For

DOI: 10.1021/acs.biochem.8b00728
Biochemistry 2018, 57, 5218−5229

Table 1. Steady-State Kinetic Parameters for Different β-Lactams with SPS-1, NDM-1, and SPM-1

	SPS-1			SPM-1[12]			NDM-1[27,28]		
substrate[a]	K_m (μM)	k_{cat} (s^{-1})	k_{cat}/K_m (s^{-1} μM^{-1})	K_m (μM)	k_{cat} (s^{-1})	k_{cat}/K_m (s^{-1} μM^{-1})	K_m (μM)	k_{cat} (s^{-1})	k_{cat}/K_m (s^{-1} μM^{-1})
chromacef	120 ± 9	2.6 ± 0.1	0.021		not available		5.1 ± 0.9	4.2	0.8
ampicillin		not observed		72 ± 3	120 ± 2	1.6	22	15	0.66
penicillin G		not observed			not available		16	11	0.68
imipenem	290 ± 50	470 ± 60	1.63	37 ± 4	33 ± 2	1	94	20	0.21
meropenem	170 ± 30	520 ± 50	3	280 ± 30	63 ± 3	0.22	49	12	0.25
cephalothin	110 ± 20	3.1 ± 0.1	0.027	4 ± 1	43 ± 2	11.7	10	4	0.4
cefuroxime		not observed		4 ± 1	37 ± 3	8.8	8	5	0.61
cephalexin		not observed			not available			not available	

[a]The buffer consisted of 50 mM HEPES (pH 7.5) containing 150 mM NaCl and 10 μM $ZnCl_2$.

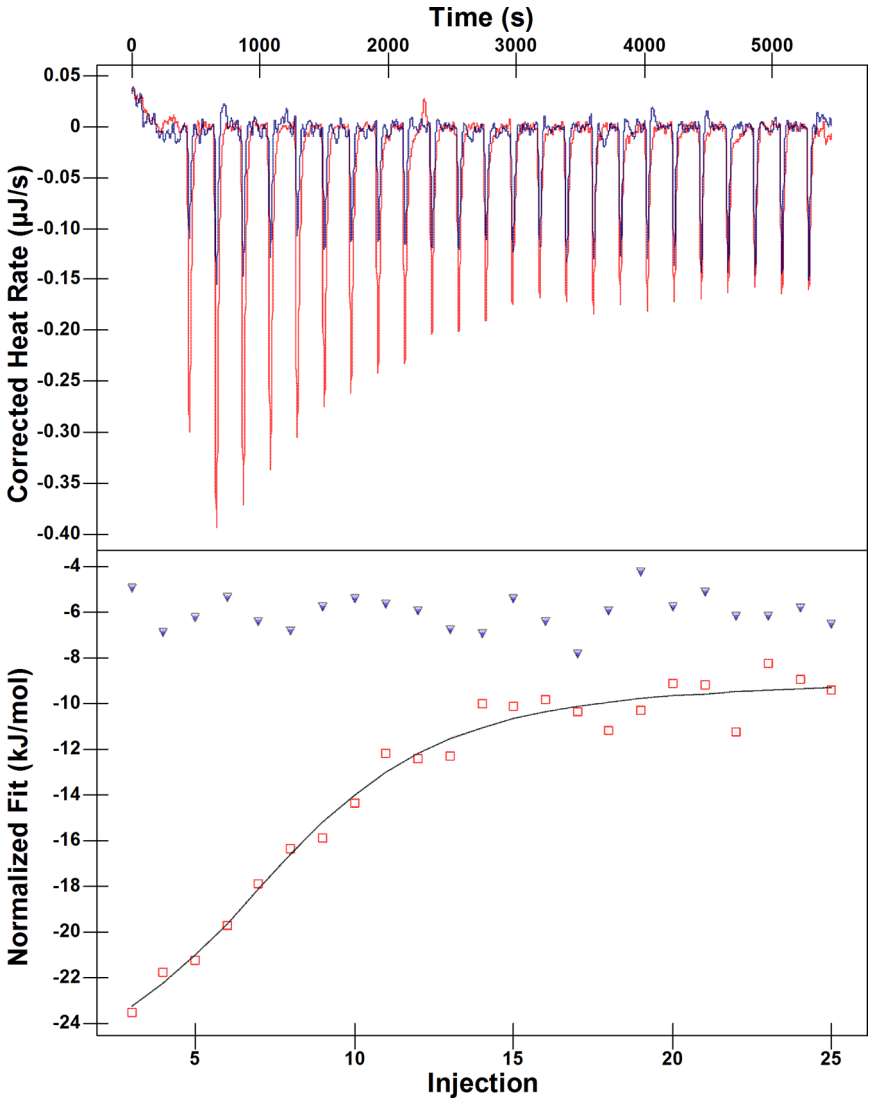

Figure 2. ITC results of L-captopril titrations with NDM-1 and SPS-1. The top panel shows the titration thermograms, and the bottom panel shows the data integration with fitted curves. Data for the NDM-1 protein are colored red, and data for SPS-1 are colored blue.

crystal harvesting, MiTeGen MicroLoops were used to harvest crystals that had been cryoprotected with LV CryoOil and then immediately frozen in liquid nitrogen. Crystals were sent to the Advanced Light Source (ALS) at Lawrence Berkeley National Laboratory where X-ray diffraction data were collected. Data were integrated and scaled using XDS[14] and SCALA.[15] Data resolution cutoffs were determined using a combination of criteria, including completeness and $CC_{1/2}$. Molecular replacement was conducted with PHASER[16] using a polyalanine search model produced from the structure of SPM-1 [Protein Data Bank (PDB) entry 4BP0].[17] The SPS-1 amino acid sequence was then docked to the molecular replacement solution. Iterative model building and refinement were conducted using COOT[18] and PHENIX[19] using isotropic individual *B* factors and TLS refinement.[20] Stereochemical and geometric quality analyses were performed with MolProbity

DOI: 10.1021/acs.biochem.8b00728
Biochemistry 2018, 57, 5218−5229

version 4.4.[21] The final model and structure factors were deposited in the Protein Data Bank as entry 6CQS.

RESULTS

Phylogenetic Analysis of SPS-1. MβLs can be grouped into three subclasses phylogenetically.[1] Subclass B1 MβLs contain a Zn_1 binding site with three histidine residues (His116, His118, and His196) and a Zn_2 site with three other residues (Asp120, Cys221, and His263).[1−3] Subclass B2 MβLs contain a Zn_1 site with one altered residue (Asn116, His118, or His196) and a Zn_2 site identical to that of the subclass B1 MβLs; the altered Zn_1 site results in B2 MβLs exhibiting activity as mononuclear Zn(II) enzymes.[22,23] The subclass B3 MβLs have a varied Zn_1 binding site (His/Gln116, His118, and His196) and a distinctive Zn_2 binding site, which does not contain a cysteine residue (Asp120, His121, and His263). To determine the phylogenetic position of SPS-1 in the classification of MβLs, phylogenetic analysis was conducted using Phylogeny.[8] The analyses showed that enzymes in subclasses B1 and B2 descended from a common ancestor and that SPS-1 was grouped in the B1 class and is highly similar to the MβL SPM-1 (Figure 1).[12] Subgroup B3 MβLs are divergent from subgroups B1 and B2.

Overexpression, Purification, and Characterization of ZnZn-SPS-1. A region of the gene for SPS-1 corresponding to residues 32−276 was synthesized to aid in cloning SPS-1 into a pET28A overexpression vector. The DNA sequence corresponding to the first 31 amino acids was not included as these residues were predicted by Phobius[24] to comprise a signal peptide. Overexpressed SPS-1 was purified with a single-step HisTrap column. TEV protease was used to remove the His_6 tag, and a second HisTrap column was used to separate SPS-1 from the cleaved tag and TEV protease. The purity of the protein was shown to be >95% by SDS−PAGE. The predicted molecular weight for tag-free SPS-1 is 27466.11 Da, as determined by the ExPASy-Compute pI/Mw tool.[10] The MALDI-TOF mass spectrum of tag-free SPS-1 showed a single peak at m/z 27469 ± 267 (Figure S1), which demonstrated that the protein was purified as a single polypeptide. The yield for tag-free SPS-1 was >20 mg of protein/L of LB medium. The tertiary structure of recombinant SPS-1 was evaluated using fluorescence spectroscopy. The resulting spectrum showed a single peak at 345 nm (excitation at 280 nm), suggesting that the majority of the protein consisted of one folded conformation (data not shown).[25] ICP-AES revealed that SPS-1 binds 1.9 ± 0.1 equiv of Zn(II), similar to the metal content of NDM-1 and other well-characterized dinuclear Zn(II)-containing MβLs.[4,26]

Steady-State Kinetics. Steady-state kinetic studies were conducted at 37 °C using chromacef, ampicillin, penicillin G, imipenem, meropenem, cephalothin, cefuroxime, and cephalexin as substrates. The resulting kinetic data are listed in Table 1. When using chromacef and cephalothin as the substrate, SPS-1 exhibited K_m values of 120 ± 9 and 110 ± 20 μM and k_{cat} values of 2.6 ± 0.1 and 3.1 ± 0.1 s^{-1}, respectively. When using imipenem and meropenem as substrates, SPS-1 exhibited K_m values of 290 ± 50 and 170 ± 30 μM and k_{cat} values of 470 ± 60 and 520 ± 50 s^{-1}, respectively. When ampicillin, penicillin G, cefuroxime, and cephalexin were used as substrates, no activity was observed. Compared to those of NDM-1 and SPM-1, the K_m values with different substrates exhibited by SPS-1 are much larger, resulting in lower catalytic efficiencies (Table 1). In contrast to most other MβLs,[1,2] SPS-1 exhibits substrate specificities for carbapenems and certain cephalosporins.

Isothermal Titration Calorimetry (ITC). ITC was used to determine if SPS-1 binds to L-captopril, which has been reported to be a competitive inhibitor of several MβLs.[29] Previous studies have shown that the S1 atom in L-captopril inserts directly between the metal ions in NDM-1,[29] displacing the bridging water/hydroxide. The crystal structure of the NDM-1/captopril complex showed that L-captopril has two binding faces: a hydrophobic face that interacts with Val73 and Met67 of the L3 loop and a hydrophilic face that hydrogen bonds to Asn220 on the L10 loop.[29] Under our experimental conditions, L-captopril binds to NDM-1 with a K_d value of 1.95 μM (Figure 2), while there is no binding between SPS-1 and L-captopril at L-captopril concentrations of ≤50 μM. This result suggests a different active site configuration in SPS-1 compared to that in NDM-1.

UV−Vis Spectroscopy. To obtain information about the metal binding sites in SPS-1, UV−vis spectra of Co(II)-substituted SPS-1 were recorded, and Co(II)-substituted NDM-1 was used as a control.[27] Metal-free SPS-1 and NDM-1 were prepared as described in Materials and Methods. TCEP was added to metal-free SPS-1, prior to adding Co(II), to prevent Co(II) oxidation.[27] Glycerol (10%) was added to the metal-free SPS-1 before Co(II) addition to prevent protein precipitation.[30] As previously reported,[26,27] Co(II)-substituted NDM-1 exhibited an intense peak at 330 nm, which was previously attributed to a Cys-S to Co(II) ligand-to-metal charge transfer transition.[31−34] The other peaks at 330, 510, 549, 615, and 640 nm (Figure 3) were assigned to ligand field

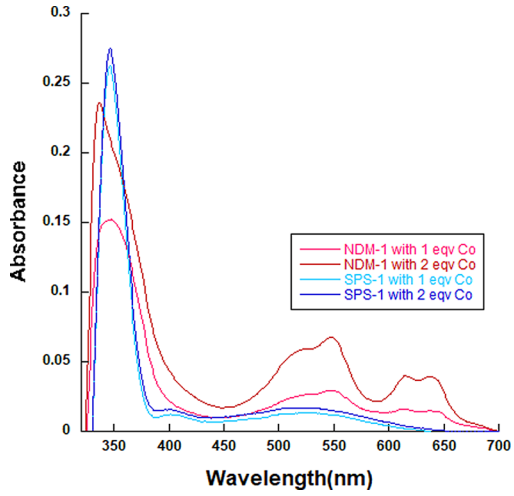

Figure 3. UV−vis spectra of apo-NDM and apo-SPS-1 treated with $CoCl_2$. The apoprotein (300 μM) with 50 mM HEPES (pH 6.8) containing 150 mM NaCl was used as a blank in this experiment.

transitions of high-spin Co(II) exhibiting a Jahn−Teller distortion.[31,35] The extinction coefficients of these ligand field transitions are consistent with one Co(II) having a coordination number of 4 and the other having a coordination number of 5.[26] Conversely, the spectra of Co(II)-substituted SPS-1 revealed a sharp absorption at 346 nm (Figure 3), suggesting a similar Zn_2 site in SPS-1 and NDM-1. However, in the spectra of Co(II)-substituted SPS-1, the ligand field transitions between 500 and 650 nm are broader and lack distinct features. Importantly, the extinction coefficient of this peak is 56 M^{-1} cm^{-1} [or ~28 M^{-1} cm^{-1} per Co(II)],

DOI: 10.1021/acs.biochem.8b00728
Biochemistry 2018, 57, 5218−5229

suggesting that both Co(II) ions are six-coordinate.[26] A similar spectrum was previously reported for Co(II)-substituted L1.[36]

NMR Spectroscopy of Co(II)-Substituted SPS-1. To further probe the metal binding sites in SPS-1, ^{1}H NMR spectra of Co(II)-substituted SPS-1 were recorded (Figure 4).

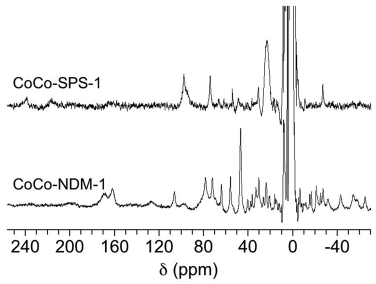

Figure 4. ^{1}H NMR (300 MHz) spectra of Co(II)-substituted NDM-1 (1 mM) and SPS-1 (0.5 mM).

As with the UV−vis spectra presented above, Co(II)-substituted NDM-1 was used as a control. Previously for Co(II)-substituted NDM-1, we showed that resonances at 64, 72, and 79 ppm are due to solvent-exchangeable protons on His120, His122, and His189 in the Zn_1 site, respectively, and resonances at 48, 107, and 165 ppm correspond to protons on Asp124, His250, and Cys208 in the Zn_2 site, respectively.[27] The spectrum of Co(II)-substituted SPS-1 revealed significant changes to the active site compared to NDM-1. Resonances at 249 and 217 ppm may be the geminal pair arising from the β-CH_2 cysteine ligand coordinating the Zn_2 site, although another weak signal was seen at 164 ppm that aligns well with the β-CH_2 cysteine protons of Co(II)-substituted NDM-1. The SPS-1 data, therefore, suggest two distinct conformations for Cys208 or that only two of the three resonances arise from Cys208.[37] Three relatively strong resonances were observed at 96, 74, and 54 ppm and can be assigned to the three Co(II)-bound histidine ligands (two from the Zn_1 site and one from the Zn_2 site). A spectrum of Co(II)-substituted SPS-1 containing 90% (v/v) D_2O was recorded to verify that these three resonances were solvent-exchangeable (Figure S2). The absence of these three resonances in the D_2O spectrum further supports the hypothesis that they arise from the three Co(II)-coordinated histidine residues. Other resonances at 31 and 23 ppm do not appear to be solvent-exchangeable and may be due to either one or both α-CH_2 aspartate protons. Of the remaining weak signals [66, 62, 48, and −27 ppm (see Figure S2)], most are likely contributions from second-sphere interactions with the metal sites. In total, these results align well with the two predicted histidine ligands at the Zn_1 site and one histidine at the Zn_2 site and show distinct differences between the active site structures of SPS-1 and NDM-1.

EPR Spectroscopy of Metal-Substituted SPS-1. Continuous wave EPR spectra of CoCo-SPS-1 and CoCo-NDM-1, obtained in both parallel and perpendicular modes, are shown in Figure 5. Both perpendicular mode spectra are typical of high-spin Co(II)-substituted metalloproteins.[38] Aside from modulation of the line shape, significant changes to the electronic environment of the Co(II) ions were not observed in these data. The sharp peak between 1600 and 1700 G in the diCo(II)-substituted NDM-1 spectrum was caused by a small fraction of Fe(III) contamination; a similar peak has been observed in previous EPR spectra of Co(II)-substituted NDM-1.[27] Co(II)-substituted NDM-1 also showed tightly coupled,

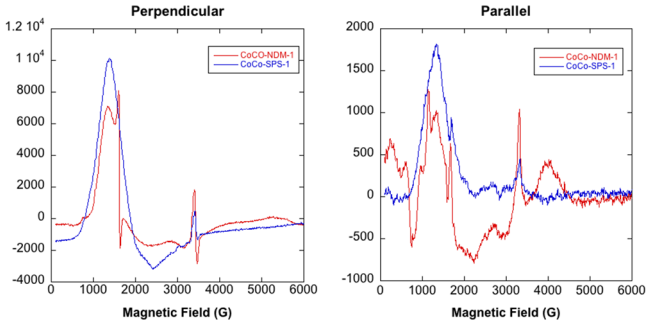

Figure 5. EPR spectra of Co(II)-substituted MβLs. Perpendicular and parallel mode, X-band EPR spectra of Co(II)-substituted NDM-1 and SPS-1. The enzyme concentration in both samples was 0.9 mM.

active site Co(II) ions in the parallel mode spectra (a deep negative feature near 800 G).[38] However, no such feature was observed in the spectrum of Co(II)-substituted SPS-1, indicating weaker coupling of active site Co(II) ions in SPS-1.

Crystal Structure of SPS-1. The structure of SPS-1 was determined to 1.70 Å resolution featuring an asymmetric unit containing a single protomer. Details of the crystallographic refinement are listed in Table 2. Two Zn(II) ions are bound in the active site, and a third zinc ion is coordinated by the side chains of the His110 and Asp106 residues of the single protomer within the asymmetric unit and the His110 and

Table 2. Crystallographic Data for SPS-1

Data Collection	
beamline	ALS 4.2.2
wavelength (Å)	1.0000
space group	$P4_32_12$
a, *b*, *c* (Å)	73.60, 73.60, 108.78
α, β, γ (deg)	90, 90, 90
resolution range[a] (Å)	34.86−1.70 (1.76−1.70)
no. of reflections[a]	157508 (6969)
no. of unique reflections[a]	33588 (3290)
completeness[a] (%)	99.95 (100.00)
Wilson *B* factor (Å^2)	19.5
$CC_{1/2}$[a]	99.5 (70.5)
Refinement	
no. of reflections[a]	33588 (3290)
PDB entry	6CQS
R_{work}/R_{free}	0.176/0.194
no. of atoms (protein/water/ligands)	1939/151/3
average *B* factor (Å^2) (protein/water/ligands)	24.9/32.9/24.5
Model Quality	
rmsd for bond lengths (Å)	0.010
rmsd for bond angles (Å)	1.073
Ramachandran favored[b] (%)	98.75
Ramachandran outliers[b] (%)	0.00
poor rotamers[b] (%)	0.00
Clash score[b]	0.78
Clash percentile[b]	99th percentile (*N* = 819; 1.70 ± 0.25 Å)
MolProbity score[b]	0.75
MolProbity score percentile[b]	100th percentile (*N* = 9248; 1.70 ± 0.25 Å)

[a]Values in parentheses are for the highest-resolution shell. [b]Values as determined by MolProbity version 4.4 (http://molprobity.biochem.duke.edu/).

DOI: 10.1021/acs.biochem.8b00728
Biochemistry 2018, 57, 5218−5229

Asp106 side chains of the $-X$, $-Y$, $-Z + 1/2$ symmetry mate. This third Zn(II) ion assists in the formation of crystal contacts and is unlikely to be physiologically relevant. The SPS-1 structure (Figure 6a,b), generated in part by Pro-origami,[39] exhibits the canonical $\alpha\beta\beta\alpha$ metallo-β-lactamase fold with two separate β-sheets and interstrand loops facilitating coordination of the active site zinc ions. SPS-1 overlays with a 0.92 Å root-mean-square deviation (rmsd) from SPM-1 for all backbone heavy atoms, indicating similar structures for both enzymes. The overlay of SPS-1 and NDM-1 is slightly poorer, exhibiting a 1.10 Å rmsd for all backbone heavy atoms. Despite a slightly worse rmsd, SPS-1 exhibits a high degree of structural similarity to both SPM-1 and NDM-1. Similar to SPM-1, SPS-1 features a pair of extended α-helices (Figure 6a,c), helices α3 and α4, located above the active site. The orientation of SPS-1 helix α3 is different in SPS-1 and SPM-1, which offers a potential avenue to the differential substrate selectivity observed for SPS-1 compared to that of SPM-1. In comparison, these helices are not found in NDM-1 (Figure 6d), and NDM-1 does not exhibit the substrate specificity observed with SPS-1. In contrast, the β-hairpin loop found in NDM-1 is significantly truncated in both SPS-1 and SPM-1. However, while the absence of corresponding helices α3 and α4 in NDM-1 expands the active site, the shortened β-hairpin loop of SPS-1 provides little in the way of expansion of the active site that could be utilized to accommodate substrates with bulky substituents as found in ampicillin, cephalexin, and cefuroxime.

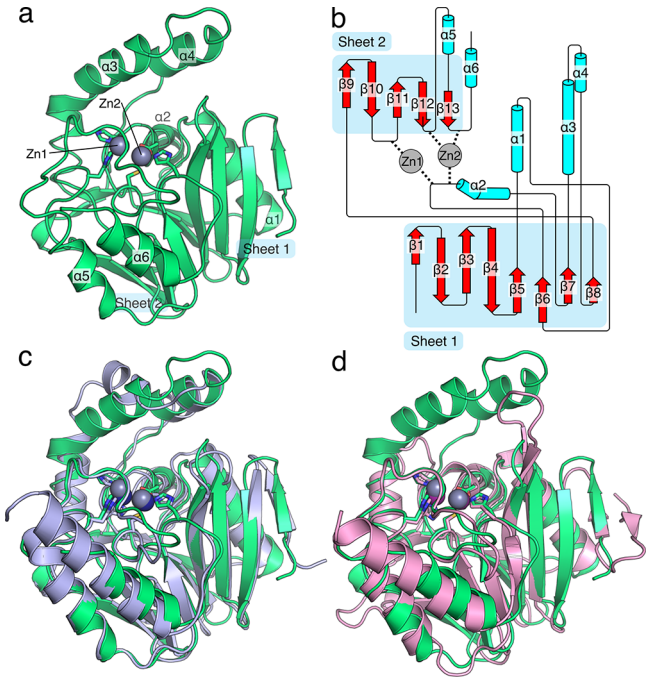

Figure 6. Overall structure of *S. smaragdinae* SPS-1. (a) The structure of SPS-1 features the canonical $\alpha\beta\beta\alpha$ metallo-β-lactamase fold with two zinc ions coordinated at the active site. Residues that coordinate zinc ions at the active site are shown as sticks, and zinc ions are shown as spheres (gray). (b) A cartoon schematic, generated in part by Pro-origami, indicates the organization of the protein and the contribution of loop residues to coordination of Zn_1 and Zn_2. (c) An overlay of SPS-1 (green) with SPM-1 (blue, PDB entry 4BP0) highlights the similar overall structure. (d) An overlay of SPS-1 (green) with NDM-1 (pink, PDB entry 4EXS) highlights a shortened SPS-1 β-hairpin loop between β-strands β3 and β4 and extended α-helices α3 and α4 above the active site for SPS-1 compared to NDM-1. For panels c and d, residues that coordinate zinc ions at the active site are shown as sticks and zinc ions are shown as spheres (SPS-1, gray; SPM-1, navy blue; NDM-1, purple).

SPS-1 Active Site. The active sites of SPS-1, SPM-1, and NDM-1 (Figure 7a) all feature two Zn(II) ions coordinated by the side chains of histidine, aspartate, or cysteine residues. The Zn_2 sites of SPS-1 (Figure 7b), SPM-1 (Figure 7c), and NDM-1 (Figure 7d) are nearly identical, each exhibiting coordination by active site histidine (SPS-1 His245, SPM-1 His258, and NDM-1 His250), aspartate (SPS-1 Asp100, SPM-1 Asp112, and NDM-1 Asp124), and cysteine (SPS-1 Cys207, SPM-1 Cys216, and NDM-1 Cys208) residues. While each protein features at least two histidine residues serving to coordinate Zn_1 (SPS-1 His98 and His188, SPM-1 His110 and His197, and NDM-1 His122 and His189), SPS-1 is missing the third coordinating histidine (SPM-1 His108 and NDM-1 His120). In the place of His108/His120, SPS-1 harbors a glycine residue (Gly96). The substitution of a glycine at this position opens up substantial space in the SPS-1 active site below Zn_1. As a result, SPS-1 features two water molecules that form a hydrogen bond network with SPS-1 active site residues. These two water molecules are featured clearly in the $2F_o - F_c$ map (Figure 8a,b) and in an omit map generated by Polder (Figure 8c,d).[40] While additional density in the omit map near Zn_1 is likely the result of truncation artifacts in the Fourier series near the zinc ions or anisotropic motion that is not readily fit by isotropic B factors, the omit map density clearly fits the proximal and distal water molecules.[41] The water molecule proximal to Gly96 is held in place by a hydrogen bond to the backbone amide proton of Tyr97 and the active site water molecule proximal to Gly96. This proximal water molecule is further anchored by a

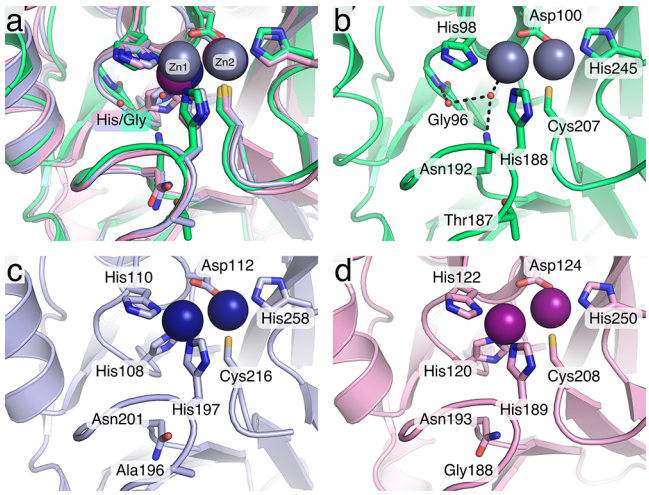

Figure 7. Organization of the *S. smaragdinae* SPS-1 active site. (a) The active sites of SPS-1 (green), SPM-1 (pink, PDB entry 4BP0), and NDM-1 (blue, PDB entry 4EXS) are shown as an overlay. (b) The active site of SPS-1 identifies a water molecule that coordinates to Zn1 in place of a histidine from the canonical HxHxD motif and a second water molecule that completes the hydrogen bond network (black dashed lines) with Gly96 and Asn192. The active sites of (c) SPM-1 and (d) NDM-1 feature the full complement of expected ligands. Throughout, key residues are shown as sticks and identified by residue name and number and zinc ions are shown as spheres (SPS-1, gray; SPM-1, navy blue; NDM-1, purple).

DOI: 10.1021/acs.biochem.8b00728
Biochemistry 2018, 57, 5218−5229

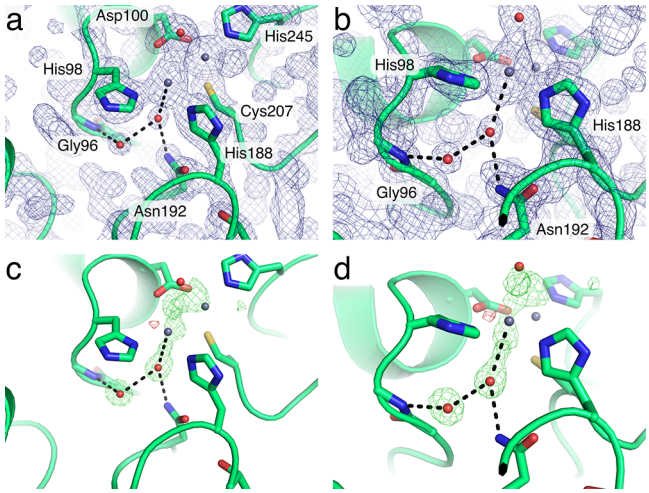

Figure 8. Electron density maps for the *S. smaragdinae* SPS-1 active site. (a and b) Two views of the SPS-1 active site with the $2F_o - F_c$ map drawn at 1.5σ. (c and d) The same views of SPS-1 are shown with an $F_o - F_c$ omit map generated by Polder drawn at ±4σ with positive density colored green and negative density colored red. Throughout, key residues are shown as sticks and water molecules (red) and zinc ions (gray) are shown as small spheres.

hydrogen bond to the side chain NH_2 of Asn192 and coordinates Zn_1. The presence of the distal and proximal water molecules is made possible by a single amino acid substitution outside the primary coordination sphere. SPS-1 Thr187 is a bulky residue in comparison to SPM-1 Ala196 and NDM-1 Gly98, which results in a change in the preferred rotamer for Asn192, thereby setting the stage for the water-mediated hydrogen bond network that situates the Gly96 distal water in position to coordinate Zn_1.

The coordinating residues and the ions in the Zn_2 sites harbor similar positions as the average distance between the Zn_2 site zinc ions across the SPS-1, SPM-1, and NDM-1 structures is 0.57 ± 0.14 Å. In comparison, an altered Zn_1 coordination sphere has a significant effect on the location of Zn_1 within the active site. The Zn_1 site for SPS-1 diverges from those observed for SPM-1, NDM-1, and all other structurally characterized metallo-β-lactamases.[1−3] While the position of Zn_2 is relatively invariant, the position of SPS-1 Zn_1 differs from those of SPM-1 Zn_1 and NDM-1 Zn_1 by 1.11 ± 0.01 Å (Figure S3). In comparison, the Zn_1 sites of SPM-1 and NDM-1 differ by only 0.43 Å. The approximately 1 Å shift of SPS-1 Zn_1 upward, away from Gly96, appears to be a direct consequence of the altered primary coordination sphere. Thus, differences in the primary (Gly96) and secondary (Thr187) coordination spheres elicit differences in the location of SPS-1 Zn_1 in comparison to SPM-1 and NDM-1.

DISCUSSION

A recent bioinformatics study revealed 279 unique, putative MβL genes, and initial biochemical and microbiological studies confirmed that 76 of the resulting proteins could be MβLs.[6] One member of this group, SPS-1 from *S. smaragdinae*, was particularly interesting because it appeared to lack the consensus HXHXD motif found in all MβLs, except those belonging to the B2 subgroup.[1−3] We were intrigued by the possibility of a novel metal binding site never before observed in the MβLs. Therefore, we endeavored to biochemically and structurally characterize SPS-1.

SPS-1 contains 276 amino acids and shares the highest degree of sequence similarity with SPM-1 from *Pseudomonas aeruginosa* (Figure 1).[12] The overlay of the SPS-1 and SPM-1 structures reveals a 0.92 Å rmsd, indicating broad structural similarity (Figure 6a,c). In addition, both SPS-1 and SPM-1 have a pair of helices located above the active site, and a similarly positioned helix is not found in NDM-1 (Figure 6a,c,d). Even though SPS-1 was sorted into the B1 phylogenetic class, it may also share some similarity with subgroup B2 MβLs, which contain one zinc in the active site (the consensus Zn_2 site) and exhibit a narrow substrate spectrum.[2] While NDM-1, VIM-2, and IMP-1 from the B1 subclass can hydrolyze penems, cephems, and carbapenems, CphA, Sfh-1, and ImiS from the B2 subclass can hydrolyze only carbapenems.[42] Surprisingly, SPS-1 exhibited significant activity against carbapenems, no activity against a penam, and weak and/or selective activity against cephem (Table 1). The most likely explanation for the absence of activity against ampicillin, penicillin G, cefuroxime, and cephalexin is steric clashes with Trp48 and Thr146 located on the extended helices α3 and α4 in SPS-1 (Figures 6, 7, and 9). Overlaying SPS-1 onto structures of NDM-1 in complex with ampicillin,[43] cephalexin,[44] and cefuroxime[44] demonstrates that the elongated α3 and α4 helices of SPS-1 block the binding of

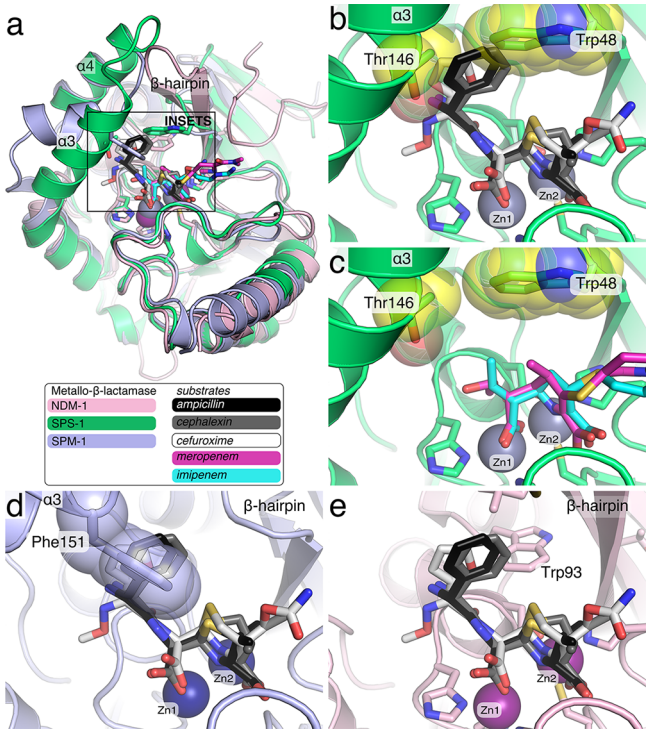

Figure 9. Overlay of *S. smaragdinae* SPS-1 and SPM-1 onto NDM-1 complexes with hydrolyzed antibiotics. The structures of SPS-1 (green, PDB entry 6CQS) and SPM-1 (light blue, PDB entry 4BP0) were superimposed onto NDM-1 (pink, PDB entry 3Q6X) with SPS-1 Zn(II) ions (gray), SPM-1 Zn(II) ions (navy blue), and NDM-1 Zn(II) ions (purple) shown as spheres. The square in panel a shows the region used for insets b−e. Hydrolyzed antibiotics determined in complex with NDM-1 are shown as sticks, including imipenem (cyan, PDB entry 5YPL), meropenem (magenta, PDB entry 5YPK), ampicillin (black, PDB entry 3Q6X), cephalexin (gray, PDB entry 4RL2), and cefuroxime (white, PDB entry 4RL0). The side chains of SPS-1 residues Thr146 and Trp48 (yellow spheres) clash with ampicillin, cephalexin, and cefuroxime.

DOI: 10.1021/acs.biochem.8b00728
Biochemistry 2018, 57, 5218−5229

substrates that contain large substituents at the 6/7 position in the β-lactam (Figure 9). Specifically, the phenyl substituents of ampicillin and cephalexin clash with both Thr146 and Trp148, while the furyl substituent of cefuroxime clashes with Thr146. While it is not surprising that the potential steric clashes (Figure 9b) correleate with the observed absence of activity by SPS-1 against position 6/7-modified penems and cephems, the structures of SPS-1 overlaid with ampicillin, cephalexin, and cefuroxime also identify steric clashes; however, Murphy et al. found that SPM-1 exhibits activity against ampicillin and cefuroxime (cephalexin was not tested).[12] The most likely explanation for the disagreement for the SPM-1 structural and activity data is that the SPM-1 structure was determined in the absence of a substrate and the conformation of the SPM-1 Phe151 side chain is a favored rotamer, **t**80°, allowed in the absence of any bound substrate. Interestingly, while electron density for the backbone of helix α3 is well-resolved for SPM-1, poor electron density for the Phe151 side chain is observed within the electron density map of 4BP0 (Figure S4). Thus, while the **t**80° Phe151 rotamer[45] modeled into the original SPM-1 crystal structure clashes with ampicillin, cephalexin, and cefuroxime (Figure 9d), altering Phe151 to adopt a different favored rotamer,[45] **m**−30°, resolves the predicted steric clash and would allow SPM-1 to bind ampicillin, cephalexin, and cefuroxime without altering the conformation of the SPM-1 backbone (Figure S4). In contrast, the backbone of SPS-1 helix α3 positions Thr146 such that all possible Thr146 side chain rotamers exhibit predicted steric clashes with ampicillin, cephalexin, and cefuroxime (Figure 9b), consistent with the observed SPS-1 substrate selectivity. Compared to the overlays with cephems and penems, overlays of SPS-1 onto structures of NDM-1 in complex with the carbapenems, imipenem[46] and meropenem[29] (Figure 9), which lack a large substituent at the 6/7 position, do not predict any steric clashes between the carbapenems and SPS-1. This is consistent with the observed activity of SPS-1 against imipenem and meropenem.

It is clear that the differences in the relative position of Zn(II) at the Zn_1 site do not in general lead to a total loss of hydrolytic activity as SPS-1 is active against antibiotics, such as meropenem, which lack the phenyl or furyl substituents found in ampicillin, cephalexin, and cefuroxime (Figure 9). Although the 1 Å displacement of Zn(II) in the Zn_1 site may also contribute to steric clash by forcing the substrate upward, this movement would only exacerbate the clashes predicted for ampicillin, cephalexin, and cefuroxime. In contrast, this 1 Å displacement of the Zn_1 site would not preclude binding of imipenem or meropenem. However, the different position and ligand environment of the Zn_1 metal ion may explain the relatively larger K_m values exhibited by SPS-1, as compared to those exhibited by NDM-1 and SPM-1 (Table 1). SPS-1 has two water molecules that form a hydrogen bond network, which accommodates the loss of a third coordinating histidine found in the Zn_1 sites of all other B1 Mβ Ls (Figure 7). For the dinuclear Zn(II)-containing Mβ Ls, substrates are thought to bind with the β-lactam carbonyl oxygen interacting with Zn_1 and the carboxylate group of the β-lactam interacting with Zn_2.[1] Therefore, the different active site geometry in SPS-1 may be the cause of the higher K_m values observed for SPS-1 against all tested substrates, reflecting weaker substrate binding to a first approximation. Altered active site geometry leading to weaker binding is also suggested by ITC studies with competitive inhibitor captopril, which show that SPS-1 does not bind captopril. These results suggest that the different position of the Zn_1 metal leads to the inability of captopril to bridge the Zn(II) ions in SPS-1. A surprising observation in the steady-state kinetic studies was that despite a different active site structure, higher k_{cat} values were exhibited by SPS-1 toward carbapenems. Given the phylogenetic grouping of SPS-1 near the B2 Mβ Ls, the positioning of the Zn_1 metal above its position in other B1 Mβ Ls, and the observed steady-state kinetic results, it is interesting to speculate that SPS-1 could be an intermediate enzyme between the dinuclear Zn(II)-containing Mβ Ls (B1's) and the mononuclear Zn(II)-containing Mβ Ls (B2's).

We have previously reported spectroscopic studies of several Co(II)-substituted Mβ Ls, including NDM-1,[27] VIM-2,[4] IMP-1,[31] L1,[36] BcI,[47] CcrA,[30] Bla2,[48] and ImiS.[22] In addition to better understanding the active sites of these enzymes, these studies have allowed us to probe the binding of metal to the Mβ Ls. Like most reported Mβ Ls, the Co(II)-substituted analogue of SPS-1 can be prepared by a direct method in which native Zn(II) is removed with a chelator and dialysis and the Co(II) analogue is prepared by adding Co(II) directly to the metal-free enzyme.[4,27] The UV−vis spectra of Co(II)-substituted SPS-1 reveal an intense peak at 346 nm, which can be attributed to a cysteine sulfur ligand-to-metal charge transfer band. The intensity of that peak is greatest when SPS-1 has 1 equiv of Co(II), demonstrating, as predicted from the crystal structure, that the first equivalent of metal binds to the Zn_2 site. The longer wavelength portion of the SPS-1 spectra is different from those of most Mβ Ls, which are often dominated by intense ligand field transitions between 450 and 600 nm from four-coordinate Co(II) in the Zn_1 site (see the control spectra of NDM-1 in Figure 3). Instead, the spectra of Co(II)-substituted SPS-1 show a broad transition in this part of the spectra, which can also be attributed to ligand field transitions. Similar spectra were reported for Mβ L L1. The intensity (ε_{525} = 56 M^{-1} cm^{-1}) of the ligand field transition(s) in Co(II)-substituted SPS-1 suggests that Co(II) in the Zn_2 site is five- or six-coordinate. The small increase in the intensity of this peak upon addition of a second equivalent of Co(II), which populates the Zn_1 site, suggests that the coordination number of Co(II) in the Zn_1 site is six.

^{1}H NMR and EPR spectra of Co(II)-substituted SPS-1 nicely correlate with the crystal structure of the Zn(II)-containing enzyme. Three solvent-exchangeable peaks can be assigned to histidine residues bound to high-spin Co(II), and other resonances, by comparison to spectra of Co(II)-containing Mβ Ls, can be assigned to cysteine and aspartate residues. The broader peaks observed in the NMR spectra of Co(II)-substituted SPS-1, as compared to those in the spectra of Co(II)-substituted NDM-1, suggest a slower T_{1e} for the unpaired electrons on Co(II) and Co(II) ions that are at best weakly spin-coupled.[49,50] The lack of spin coupling is clearly observed in the parallel mode EPR spectra of Co(II)-substituted SPS-1. The positioning of the metal ion in the Zn_1 site is most likely the cause of the loss of coupling and nicely explains the lack of binding by captopril.

An intriguing question regarding SPS-1 is why *S. smaragdinae*, specifically strain SEBR 4228^T from a water sample near a Congo offshore oilfield, produces an Mβ L. Spirochetes are spiral-shaped bacteria and are pathogenic, causing yaws, Lyme disease, relapsing fever, and syphilis.[51] One common treatment for some spirochete infections is the administration of β-lactams,[52] and it is possible that another spirochete strain transferred resistance to *S. smaragdinae* strain

DOI: 10.1021/acs.biochem.8b00728
Biochemistry 2018, 57, 5218−5229

SEBR 4228^T. SPS-1 from *S. smaragdinae* has not been identified in any patients, and there are no reports of any human infections caused by *S. smaragdinae*. According to Hatosy,[53] there are four possible mechanisms to explain how bacteria in the ocean gain antibiotic resistance. The first prediction is that antibiotic-resistant bacteria migrate from land into marine environments. The second prediction is that antibiotics enter into the marine environment, causing bacteria to evolve antibiotic-resistant phenotypes. However, both of these mechanisms seem unlikely because of the dilution of the bacteria and antibiotics by the ocean. The third prediction is that antimicrobial compounds are being produced *in situ* by marine organisms, potentially to give these organisms a survival advantage. The fourth prediction is that the proteins conferring antibiotic resistance phenotypes mutated from a protein that has a different function *in vivo*. SPS-1, like other MβLs, adopts a characteristic $\alpha\beta\beta\alpha$ fold. This $\alpha\beta\beta\alpha$ fold is found in a larger superfamily of metalloenzymes, such as glyoxalase II, arylsulfatase, and RNA-processing enzymes,[54,55] with diverse biological functions. It is important to note that the evolution of one of these enzymes into a MβL would likely require the presence of β-lactams to drive evolution.

CONCLUSIONS

Despite the question of why this spirochete produces a MβL, SPS-1 is a unique MβL with a novel metal binding site. SPS-1 exhibits substrate specificity similar to that of the B2 MβLs, yet SPS-1 can hydrolyze β-lactams other than carbapenems. The novel ligand set for the SPS-1 active site provides a glimpse at possible mutations in B1 MβLs that can still allow for β-lactam hydrolysis, suggesting that broader diversity is possible for this family of enzymes. The uncoupling of the Zn_1 and Zn_2 metal sites identifies SPS-1 as a possible intermediate between the dinuclear Zn(II)-containing B1 MβLs and mononuclear Zn(II)-containing B2-MβLs. Additional studies are needed to better understand how the different metal center in SPS-1 might affect the mechanism of β-lactam hydrolysis and the interaction with current and future inhibitor scaffolds.

ASSOCIATED CONTENT

Supporting Information

The Supporting Information is available free of charge on the ACS Publications website at DOI: 10.1021/acs.biochem.8b00728.

Four supplemental figures (PDF)

AUTHOR INFORMATION

Corresponding Authors

*Department of Chemistry and Biochemistry, Miami University, 651 E. High Street, 160 Hughes Laboratories, Oxford, OH 45056. E-mail: crowdemw@MiamiOH.edu. Telephone: (513) 529-2813. Fax: (513) 529-5715.

*E-mail: pagerc@MiamiOH.edu.

ORCID

Stacey Lowery Bretz: 0000-0001-5503-8987

Robert A. Bonomo: 0000-0002-3299-894X

Richard C. Page: 0000-0002-3006-3171

Michael W. Crowder: 0000-0002-3138-0283

Author Contributions

Cloning, protein expression and purification, ITC, and fluorescence experiments were conducted by Z.C., C.M., K.M., E.C., H.Z., R.L.K., and S.F. X-ray crystallography data collection and structure solution were performed by J.V., J.C.N., and R.C.P. M.W.C. and R.C.P. drafted the manuscript with input from their co-authors. All authors approved the final version of the manuscript.

Funding

The authors acknowledge funding from the National Institutes of Health (R01 GM111926 to D.L.T., R.A.B., R.C.P., and M.W.C.; R35 GM128595 to R.C.P.; R01AI100560 to R.A.B.; R01AI063517 to R.A.B.; and R01AI072219 to R.A.B.). M.W.C. and D.L.T. acknowledge support from the National Science Foundation (CHE-1509285). R.C.P. acknowledges support from Miami University through the Robert H. and Nancy J. Blayney Professorship. The Advanced Light Source is supported by the U.S. Department of Energy under Contract DE-AC03-76SF00098 at Lawrence Berkeley National Laboratory. This study was supported in part by funds and/or facilities provided by the Cleveland Department of Veterans Affairs, Award 1I01BX001974 (to RAB) from the Biomedical Laboratory Research & Development Service of the VA Office of Research and Development and the Geriatric Research Education and Clinical Center VISN 10 (to RAB).

Notes

The authors declare no competing financial interest.

ABBREVIATIONS

EPR, electron paramagnetic resonance; IPTG, isopropyl β-D-1-thiogalactopyranoside; ITC, isothermal titration calorimetry; MβL, metallo-β-lactamase; NDM, New Delhi MβL; NMR, nuclear magnetic resonance; SDS−PAGE, sodium dodecyl sulfate−polyacrylamide gel electrophoresis; TCEP, tris(2-carboxyethyl)phosphine hydrochloride; TEV, tobacco etch virus.

REFERENCES

(1) Palzkill, T. (2013) Metallo-beta-lactamase structure and function. *Ann. N. Y. Acad. Sci. 1277*, 91−104.

(2) Meini, M. R., Llarrull, L. I., and Vila, A. J. (2015) Overcoming differences: The catalytic mechanism of metallo-beta-lactamases. *FEBS Lett. 589*, 3419−3432.

(3) Mojica, M. F., Bonomo, R. A., and Fast, W. (2016) B1-Metallo-beta-Lactamases: Where Do We Stand? *Curr. Drug Targets 17*, 1029−1050.

(4) Aitha, M., Marts, A. R., Bergstrom, A., Møller, A. J., Moritz, L., Turner, L., Nix, J. C., Bonomo, R. A., Page, R. C., Tierney, D. L., and Crowder, M. W. (2014) Biochemical, mechanistic, and spectroscopic characterization of metallo-beta-lactamase VIM-2. *Biochemistry 53*, 7321−7331.

(5) Martinez, J. L. (2008) Antibiotics and antibiotic resistance genes in natural environments. *Science 321*, 365−367.

(6) Berglund, F., Marathe, N. P., Osterlund, T., Bengtsson-Palme, J., Kotsakis, S., Flach, C. F., Larsson, D. G. J., and Kristiansson, E. (2017) Identification of 76 novel B1 metallo-beta-lactamases through large-scale screening of genomic and metagenomic data. *Microbiome 5*, 134.

(7) Mavromatis, K., Yasawong, M., Chertkov, O., Lapidus, A., Lucas, S., Nolan, M., Del Rio, T. G., Tice, H., Cheng, J. F., Pitluck, S., Liolios, K., Ivanova, N., Tapia, R., Han, C., Bruce, D., Goodwin, L., Pati, A., Chen, A., Palaniappan, K., Land, M., Hauser, L., Chang, Y. J., Jeffries, C. D., Detter, J. C., Rohde, M., Brambilla, E., Spring, S., Goker, M., Sikorski, J., Woyke, T., Bristow, J., Eisen, J. A., Markowitz, V., Hugenholtz, P., Klenk, H. P., and Kyrpides, N. C. (2010) Complete genome sequence of Spirochaeta smaragdinae type strain (SEBR 4228). *Stand. Genomic Sci. 3*, 136−144.

(8) Dereeper, A., Guignon, V., Blanc, G., Audic, S., Buffet, S., Chevenet, F., Dufayard, J. F., Guindon, S., Lefort, V., Lescot, M.,

DOI: 10.1021/acs.biochem.8b00728
Biochemistry 2018, 57, 5218−5229

Claverie, J. M., and Gascuel, O. (2008) Phylogeny.fr: robust phylogenetic analysis for the non-specialist. *Nucleic Acids Res. 36*, W465−469.
(9) Dereeper, A., Audic, S., Claverie, J. M., and Blanc, G. (2010) BLAST-EXPLORER helps you building datasets for phylogenetic analysis. *BMC Evol. Biol. 10*, 8.
(10) Wilkins, M. R., Gasteiger, E., Bairoch, A., Sanchez, J. C., Williams, K. L., Appel, R. D., and Hochstrasser, D. F. (1998) Protein identification and analysis tools in the ExPASy server. *Methods Mol. Biol. 112*, 531−552.
(11) Beavis, R. C., Chait, B. T., and Fales, H. M. (1989) Cinnamic acid derivatives as matrices for ultraviolet laser desorption mass spectrometry of proteins. *Rapid Commun. Mass Spectrom. 3*, 432−435.
(12) Murphy, T. A., Simm, A. M., Toleman, M. A., Jones, R. N., and Walsh, T. R. (2003) Biochemical characterization of the acquired metallo-beta-lactamase SPM-1 from Pseudomonas aeruginosa. *Antimicrob. Agents Chemother. 47*, 582−587.
(13) Riley, E. A., Petros, A. K., Smith, K. A., Gibney, B. R., and Tierney, D. L. (2006) Frequency-switching inversion-recovery for severely hyperfine-shifted NMR: evidence of asymmetric electron relaxation in high-spin Co(II). *Inorg. Chem. 45*, 10016−10018.
(14) Kabsch, W. (2010) Xds. *Acta Crystallogr., Sect. D: Biol. Crystallogr. 66*, 125−132.
(15) Evans, P. (2006) Scaling and assessment of data quality. *Acta Crystallogr., Sect. D: Biol. Crystallogr. 62*, 72−82.
(16) McCoy, A. J., Grosse-Kunstleve, R. W., Adams, P. D., Winn, M. D., Storoni, L. C., and Read, R. J. (2007) Phaser crystallographic software. *J. Appl. Crystallogr. 40*, 658−674.
(17) Brem, J., Struwe, W. B., Rydzik, A. M., Tarhonskaya, H., Pfeffer, I., Flashman, E., van Berkel, S. S., Spencer, J., Claridge, T. D., McDonough, M. A., Benesch, J. L., and Schofield, C. J. (2015) Studying the active-site loop movement of the Sao Paolo metallo-beta-lactamase-1. *Chem. Sci. 6*, 956−963.
(18) Emsley, P., Lohkamp, B., Scott, W. G., and Cowtan, K. (2010) Features and development of Coot. *Acta Crystallogr., Sect. D: Biol. Crystallogr. 66*, 486−501.
(19) Adams, P. D., Afonine, P. V., Bunkoczi, G., Chen, V. B., Davis, I. W., Echols, N., Headd, J. J., Hung, L. W., Kapral, G. J., Grosse-Kunstleve, R. W., McCoy, A. J., Moriarty, N. W., Oeffner, R., Read, R. J., Richardson, D. C., Richardson, J. S., Terwilliger, T. C., and Zwart, P. H. (2010) PHENIX: a comprehensive Python-based system for macromolecular structure solution. *Acta Crystallogr., Sect. D: Biol. Crystallogr. 66*, 213−221.
(20) Painter, J., and Merritt, E. A. (2006) Optimal description of a protein structure in terms of multiple groups undergoing TLS motion. *Acta Crystallogr., Sect. D: Biol. Crystallogr. 62*, 439−450.
(21) Chen, V. B., Arendall, W. B., 3rd, Headd, J. J., Keedy, D. A., Immormino, R. M., Kapral, G. J., Murray, L. W., Richardson, J. S., and Richardson, D. C. (2010) MolProbity: all-atom structure validation for macromolecular crystallography. *Acta Crystallogr., Sect. D: Biol. Crystallogr. 66*, 12−21.
(22) Sharma, N. P., Hajdin, C., Chandrasekar, S., Bennett, B., Yang, K. W., and Crowder, M. W. (2006) Mechanistic studies on the mononuclear ZnII-containing metallo-beta-lactamase ImiS from Aeromonas sobria. *Biochemistry 45*, 10729−10738.
(23) Bebrone, C., Delbruck, H., Kupper, M. B., Schlomer, P., Willmann, C., Frere, J. M., Fischer, R., Galleni, M., and Hoffmann, K. M. V. (2009) The Structure of the Dizinc Subclass B2 Metallo-beta-Lactamase CphA Reveals that the Second Inhibitory Zinc Ion Binds in the Histidine Site. *Antimicrob. Agents Chemother. 53*, 4464−4471.
(24) Kall, L., Krogh, A., and Sonnhammer, E. L. (2007) Advantages of combined transmembrane topology and signal peptide prediction–the Phobius web server. *Nucleic Acids Res. 35*, W429−432.
(25) Hu, Z., Periyannan, G. R., and Crowder, M. W. (2008) Folding strategy to prepare Co(II)-substituted metallo-beta-lactamase L1. *Anal. Biochem. 378*, 177−183.
(26) Thomas, P. W., Zheng, M., Wu, S., Guo, H., Liu, D., Xu, D., and Fast, W. (2011) Characterization of purified New Delhi metallo-beta-lactamase-1. *Biochemistry 50*, 10102−10113.
(27) Yang, H., Aitha, M., Marts, A. R., Hetrick, A., Bennett, B., Crowder, M. W., and Tierney, D. L. (2014) Spectroscopic and mechanistic studies of heterodimetallic forms of metallo-beta-lactamase NDM-1. *J. Am. Chem. Soc. 136*, 7273−7285.
(28) Yong, D., Toleman, M. A., Giske, C. G., Cho, H. S., Sundman, K., Lee, K., and Walsh, T. R. (2009) Characterization of a new metallo-beta-lactamase gene, bla(NDM-1), and a novel erythromycin esterase gene carried on a unique genetic structure in Klebsiella pneumoniae sequence type 14 from India. *Antimicrob. Agents Chemother. 53*, 5046−5054.
(29) King, D. T., Worrall, L. J., Gruninger, R., and Strynadka, N. C. (2012) New Delhi metallo-beta-lactamase: structural insights into beta-lactam recognition and inhibition. *J. Am. Chem. Soc. 134*, 11362−11365.
(30) Periyannan, G. R., Costello, A. L., Tierney, D. L., Yang, K. W., Bennett, B., and Crowder, M. W. (2006) Sequential binding of cobalt(II) to metallo-beta-lactamase CcrA. *Biochemistry 45*, 1313−1320.
(31) Griffin, D. H., Richmond, T. K., Sanchez, C., Møller, A. J., Breece, R. M., Tierney, D. L., Bennett, B., and Crowder, M. W. (2011) Structural and kinetic studies on metallo-beta-lactamase IMP-1. *Biochemistry 50*, 9125−9134.
(32) Orellano, E. G., Girardini, J. E., Cricco, J. A., Ceccarelli, E. A., and Vila, A. J. (1998) Spectroscopic characterization of a binuclear metal site in Bacillus cereus beta-lactamase II. *Biochemistry 37*, 10173−10180.
(33) Wang, Z., and Benkovic, S. J. (1998) Purification, characterization, and kinetic studies of a soluble Bacteroides fragilis metallo-beta-lactamase that provides multiple antibiotic resistance. *J. Biol. Chem. 273*, 22402−22408.
(34) Crowder, M. W., Yang, K. W., Carenbauer, A. L., Periyannan, G., Seifert, M. E., Rude, N. E., and Walsh, T. R. (2001) The problem of a solvent exposable disulfide when preparing Co(II)-substituted metallo-beta-lactamase L1 from Stenotrophomonas maltophilia. *JBIC, J. Biol. Inorg. Chem. 6*, 91−99.
(35) Garmer, D. R., and Krauss, M. (1993) Ab initio quantum chemical study of the cobalt d-d spectroscopy of several substituted zinc enzymes. *J. Am. Chem. Soc. 115*, 10247−10257.
(36) Hu, Z., Periyannan, G., Bennett, B., and Crowder, M. W. (2008) Role of the Zn1 and Zn2 sites in metallo-beta-lactamase L1. *J. Am. Chem. Soc. 130*, 14207−14216.
(37) Bergstrom, A., Katko, A., Adkins, Z., Hill, J., Cheng, Z. S., Burnett, M., Yang, H., Aitha, M., Mehaffey, M. R., Brodbelt, J. S., Tehrani, K. H. M. E., Martin, N. I., Bonomo, R. A., Page, R. C., Tierney, D. L., Fast, W., Wright, G. D., and Crowder, M. W. (2018) Probing the Interaction of Aspergillomarasmine A with Metallo-beta-lactamases NDM-1, VIM-2, and IMP-7. *ACS Infect. Dis. 4*, 135−145.
(38) Bennett, B. (2010) EPR of Cobalt-Substituted Zinc Enzymes. In *Metals in Biology: Applications of High Resolution EPR to Metalloenzymes* (Berliner, G. H. L., Ed.) pp 345−370, Springer, New York.
(39) Stivala, A., Wybrow, M., Wirth, A., Whisstock, J. C., and Stuckey, P. J. (2011) Automatic generation of protein structure cartoons with Pro-origami. *Bioinformatics 27*, 3315−3316.
(40) Liebschner, D., Afonine, P. V., Moriarty, N. W., Poon, B. K., Sobolev, O. V., Terwilliger, T. C., and Adams, P. D. (2017) Polder maps: improving OMIT maps by excluding bulk solvent. *Acta Crystallogr. D Struct Biol. 73*, 148−157.
(41) Read, R. (2013) *Advancing methods for biomolecular crystallography*, Springer, New York.
(42) Wommer, S., Rival, S., Heinz, U., Galleni, M., Frere, J. M., Franceschini, N., Amicosante, G., Rasmussen, B., Bauer, R., and Adolph, H. W. (2002) Substrate-activated zinc binding of metallo-beta -lactamases: physiological importance of mononuclear enzymes. *J. Biol. Chem. 277*, 24142−24147.
(43) Zhang, H., and Hao, Q. (2011) Crystal structure of NDM-1 reveals a common beta-lactam hydrolysis mechanism. *FASEB J. 25*, 2574−2582.

DOI: 10.1021/acs.biochem.8b00728
Biochemistry 2018, 57, 5218−5229

(44) Feng, H., Ding, J. J., Zhu, D. Y., Liu, X. H., Xu, X. Y., Zhang, Y., Zang, S. S., Wang, D. C., and Liu, W. (2014) Structural and Mechanistic Insights into NDM-1 Catalyzed Hydrolysis of Cephalosporins. *J. Am. Chem. Soc. 136*, 14694−14697.
(45) Lovell, S. C., Word, J. M., Richardson, J. S., and Richardson, D. C. (2000) The penultimate rotamer library. *Proteins: Struct., Funct., Genet. 40*, 389−408.
(46) Feng, H., Liu, X., Wang, S., Fleming, J., Wang, D.-C., and Liu, W. (2017) The mechanism of NDM-1-catalyzed carbapenem hydrolysis is distinct from that of penicillin or cephalosporin hydrolysis. *Nat. Commun. 8*, 2242.
(47) Breece, R. M., Llarrull, L. I., Tioni, M. F., Vila, A. J., and Tierney, D. L. (2012) X-ray absorption spectroscopy of metal site speciation in the metallo-beta-lactamase BcII from Bacillus cereus. *J. Inorg. Biochem. 111*, 182−186.
(48) Hawk, M. J., Breece, R. M., Hajdin, C. E., Bender, K. M., Hu, Z., Costello, A. L., Bennett, B., Tierney, D. L., and Crowder, M. W. (2009) Differential binding of Co(II) and Zn(II) to metallo-beta-lactamase Bla2 from Bacillus anthracis. *J. Am. Chem. Soc. 131*, 10753−10762.
(49) Holz, R. C., Bennett, B., Chen, G. J., and Ming, L. J. (1998) Proton NMR spectroscopy as a probe of dinuclear copper(II) active sites in metalloproteins. Characterization of the hyperactive copper-(II)-substituted aminopeptidase from Aeromonas proteolytica. *J. Am. Chem. Soc. 120*, 6329−6335.
(50) Brink, J. M., Rose, R. A., and Holz, R. C. (1996) Characterization of the structural and electronic properties of spin-coupled dinuclear copper(II) centers by proton NMR spectroscopy. *Inorg. Chem. 35*, 2878−2885.
(51) Wolgemuth, C. W. (2015) Flagellar motility of the pathogenic spirochetes. *Semin. Cell Dev. Biol. 46*, 104−112.
(52) Dassanayake, R. P., Sarath, G., and Duhamel, G. E. (2005) Penicillin-binding proteins in the pathogenic intestinal spirochete Brachyspira pilosicoli. *Antimicrob. Agents Chemother. 49*, 1561−1563.
(53) Hatosy, S. M., and Martiny, A. C. (2015) The Ocean as a Global Reservoir of Antibiotic Resistance Genes. *Appl. Environ. Microbiol. 81*, 7593−7599.
(54) Daiyasu, H., Osaka, K., Ishino, Y., and Toh, H. (2001) Expansion of the zinc metallo-hydrolase family of the beta-lactamase fold. *FEBS Lett. 503*, 1−6.
(55) Pettinati, I., Brem, J., Lee, S. Y., McHugh, P. J., and Schofield, C. J. (2016) The Chemical Biology of Human Metallo-beta-Lactamase Fold Proteins. *Trends Biochem. Sci. 41*, 338−355.

DOI: 10.1021/acs.biochem.8b00728
Biochemistry 2018, 57, 5218−5229